Journal of Hydrology 526 (2015) 253–264

Contents lists available at ScienceDirect

Journal of Hydrology

journal homepage: www.elsevier.com/locate/jhydrol

Spatio-temporal variation of drought in China during 1961–2012: A climatic perspective

Kai Xu [a], Dawen Yang [a,*], Hanbo Yang [a], Zhe Li [a], Yue Qin [a], Yan Shen [b]

[a] State Key Laboratory of Hydroscience and Engineering, Department of Hydraulic Engineering, Tsinghua University, Beijing 100084, China
[b] National Meteorological Information Center, China Meteorological Administration, Beijing 100084, China

ARTICLE INFO

Article history:
Available online 30 September 2014

Keywords:
Drought index
Spatio-temporal variation
Drought identification
China

SUMMARY

Understanding the spatial and temporal variation of drought is essentially important in drought assessment. In most previous studies, drought event is usually identified in space and time separately, ignoring the nature of the dynamic processes. In order to better understand how drought changes have taken place in China during the past half-century, we carried out a comprehensive analysis of their spatio-temporal variation based on multiple drought indices from a climatic perspective. A 3-dimensional clustering method is developed to identify drought events in China from 1961 to 2012 based on the 0.25° gridded indices of SPI3 (3 months Standardized Precipitation Index), RDI3 (3 months Reconnaissance Drought Index) and SPEI3 (3 months Standardized Precipitation Evapotranspiration Index). Drought events are further characterized by five parameters: duration, affected area, severity, intensity, and centroid. Remotely sensed soil moisture data were used to validate the rationality of identified drought events. The results show that the two most severe drought events in the past half century which occurred in the periods 1962–1963 and 2010–2011 swept more than half of the non-arid regions in China. Large magnitude droughts were usually centered in the region from North China Plain to the downstream of Yangtze River. The western part of North China Plain, Loess Plateau, Sichuan Basin and Yunnan-Guizhou Plateau had a significant drying trend, which is mainly caused by the significant decrease of precipitation. The three drought indices have almost the same performance in the humid regions, while SPI and RDI were found to be more appropriate than SPEI in the arid regions.

1. Introduction

Drought is a natural phenomenon in which the natural water availability for a region is lower than that under normal conditions for a prolonged period. It may last for weeks, months, years or even decades. Drought is one of the costliest and most widespread natural disasters (Wilhite, 2000; Bryant, 2005) that may have devastating impacts on agriculture, water resources, environment and human lives. Droughts occur over most parts of the world, both in wet and humid regions (Dai, 2011). Understanding the spatial and temporal variations of drought is of primary importance for freshwater planning and management (Mishra and Singh, 2010).

Due to the monsoon climate interacted with the complicated geographical landscapes, severe drought of high frequency is one of the most devastating natural disasters in China. According to statistics, the drought affected area and drought damaged area have greatly increased in the past 50 years (Wang et al., 2012). In the 2000s, extreme droughts occurred frequently in China, for example, the winter–spring drought in southwest China during 2009–2010 (Lu et al., 2011; Zhang et al., 2012a; Zhao et al., 2013) and the spring–summer drought over the middle and lower reaches of Yangtze River in 2011 (Lu et al., 2013). They brought significant socio-economic and eco-environment damages. China is facing an increasing drought risk in the 21st century under the changing climate. Better understanding of the drought changes in the past is important for managing the future drought risk.

1.1. Drought index and drought identification

Drought is monitored and quantified by drought indices, and various indices have been developed to depict the drought in different applications (Dracup et al., 1980; Wilhite and Glantz, 1985). Among these indices, the standardized precipitation index (SPI; McKee et al., 1993) is the most popular one. SPI has the advantages of flexible time scale and simple calculation procedure. However, SPI also has disadvantages; it only utilizes precipitation information, without considering other meteorological variables that play

* Corresponding author.
E-mail address: yangdw@tsinghua.edu.cn (D. Yang).

http://dx.doi.org/10.1016/j.jhydrol.2014.09.047
0022-1694/

important roles during the development of a drought event (Taylor et al., 2012; Teuling et al., 2013). Recently, many attempts have been made to improve SPI by incorporating other hydrometeorological variables. Tsakiris et al. (2007) proposed the Reconnaissance Drought Index (RDI) based on the quotient of cumulative precipitation and cumulative potential evapotranspiration following the same methodology as with SPI. Vicente-Serrano et al. (2010) developed the standardized precipitation evapotranspiration index (SPEI), defined as the difference between the cumulative precipitation and the cumulative potential evapotranspiration, and found that it is sensitive to the temperature. In China, China Meteorological Administration (CMA) uses the meteorological composite index (CI) for drought monitoring, which is a combination of one-month SPI, 3 month SPI and monthly relative humidity index (P/E_p) (CMA, 2006). Ma et al. (2013) formulated the standardized Palmer drought index (SPDI) by combining the methodology of PDSI (Palmer Drought Severity Index; Palmer, 1965) and SPI. Kao and Govindaraju (2010) proposed the joint drought index (JDI) based on the joint distribution of accumulated precipitation and streamflow using copulas. Following the framework similar to that of JDI, Hao and AghaKouchak (2013) proposed the multivariate standardized drought index (MSDI) by combining accumulated precipitation and soil moisture. However, there have been only a few studies (Guttman, 1998; Khalili et al., 2011; Vicente-Serrano et al., 2012) carried out for the inter-comparison among the different drought indices.

Drought identification and characterization is a pre-requisite to spatial and temporal variation analysis and drought frequency analysis. In general, drought is often characterized by its duration, severity, intensity and spatial extent. Yevjevich (1967) proposed the one-dimensional truncation method to extract drought duration, severity, and intensity from drought index sequence. Statistical methods, such as wavelet analysis (Min et al., 2003), empirical orthogonal functions (Kim et al., 2011; Song et al., 2013), principal component analysis (PCA) and cluster analysis (Chen and Yang, 2012; Gocic and Trajkovic, 2014), Shannon entropy (She and Xia, 2012) have been widely employed to estimate the spatial pattern of drought. All these methods discard much of the spatio-temporal information by reducing drought events to a lower-order subspace (Lloyd-Hughes, 2012), thereby not enabling to capture the real drought structure in space–time dimensions. Meanwhile, many other studies have been devoted to identification of drought event based on image recognition methods. For example, Andreadis et al. (2005) proposed a clustering algorithm to extract the voxels of drought connected in space and time. Lloyd-Hughes (2012) extended the clustering algorithm to 3-dimensional space (longitude, latitude, and time), fulfilled the complete spatio-temporal representation of the drought event. However, these methods have been barely used in drought assessments due to their complexity.

1.2. Previous studies on China drought

In the context of climate change, the spatial and temporal variation of drought ranging from regional to national scale has become a research hot topic in China. The previous studies of drought during the past decades using SPI showed that the eastern part of China being far more hazardous than the western part (He et al., 2011); north Xinjiang had a decreasing trend of drought severity (Zhang et al., 2012b); severe drought increased gradually over China, while rapidly increased in southwest China (Yang et al., 2013). It was found that positive feedback from low precipitation and high temperature maintained the severe drought during 2009–2010 in southwest China (Lu et al., 2011; Zhang et al., 2012a; Zhao et al., 2013). Therefore, the temperature is also incorporated into the drought assessment. Based on the commonly used drought index CI, Yu et al. (2013) found that the drought frequency was lower in summer and autumn, and higher in winter and spring over southwest China; Song et al. (2013) evaluated the spatial and temporal distribution of drought over the Songnen Plain of northeast China; Qian et al. (2011) ranked regional drought events from 1960 to 2009, and found that droughts frequently occurred in Southwest China and the Yellow River basin. Yu et al. (2014) used the SPEI index and reported that drought was becoming more severe since late 1990s for most parts of China, and the drying area increased by 3.72% per decade. Using the land surface model simulated soil moisture, Wang et al. (2011) quantified drought in China during 1950–2006 and found that central and northeastern China had significant drying trend, whereas Xinjiang and Tibetan Plateau showed significant wetting trend, and the drying area was larger than the wetting area; Wu et al. (2011) found a significant increasing trend of drought occurrence frequency, particularly in north China.

Although such a variety of studies have focused on the spatial and temporal variation of drought in China, yet the methods used for drought identification in previous studies were always simplified to a lower dimension. Consequently drought variations were analyzed in time and space separately, either the time evolution of drought over a fixed area or the drought spatial patterns at a certain time. These simplified methods are inadequate to describe the spatio-temporal structure of drought. Therefore, it is necessary to identify and characterize drought events in a 3-dimensional framework for a better understanding of the spatio-temporal variation. Furthermore, the inter-comparison among the different drought indices was rarely done in previous studies.

1.3. Objectives and structure of this study

The present study focusses on the long-term drought assessment in China using a 3-dimensional identification and characterization approach in a multi-metric framework. It aims to evaluate spatio-temporal variation of drought during the past half century. Firstly, three most widely used meteorological drought indices, namely SPI, RDI, and SPEI were calculated. Then, the 3-D drought identification method was adopted to identify the drought events based on these three indices. Finally, the spatial and temporal variation of drought events in the past 52 years were analyzed.

The remaining parts of this paper are organized as follows. Section 2 describes the data sets and methodology used. Section 3 presents the validation of identified drought events and their spatio-temporal variations. Section 4 discusses drought trend influenced by precipitation and potential evaporation, and the disadvantages of the climatic drought indices. Finally, some conclusions are given in Section 5.

2. Data and methodology

2.1. Data and study area

Daily gridded ($0.25^\circ \times 0.25^\circ$) precipitation data from 1960 to 2012 were acquired from National Meteorological Information Center (NMIC). They are generated from observations of over 2419 national-level gauges, interpolated using the kernel interpolation algorithm controlled by the background climatology fields. Absolute error of 91% of the data set is less than 0.1 mm/day, meaning this data set can capture the rainfall temporal process and spatial distribution accurately (Shen et al., 2010). The gridded precipitation data was integrated into the monthly scale for the drought analysis.

To calculate the potential evaporation (E_p), daily meteorological data set, including air temperature (T), wind speed, relative humidity, sunshine time, and pressure from 743 gauges (see Fig. 1) over

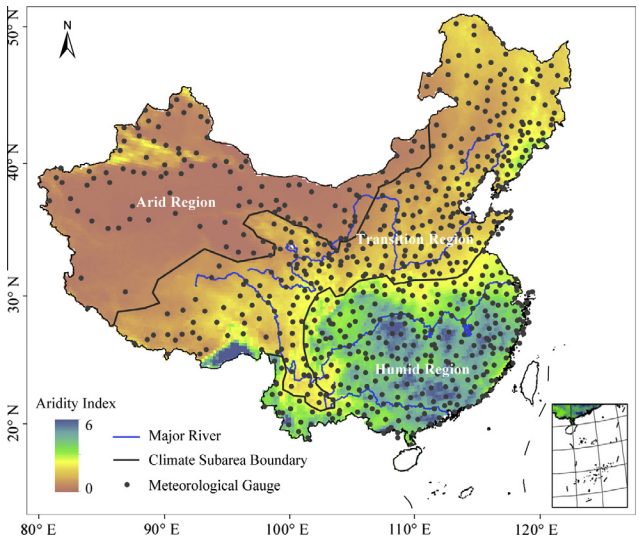

Fig. 1. Locations of national meteorological stations and climatic sub-regions in China mainland.

the period 1960–2012 were acquired from the China Meteorological Administration (CMA). The gauge data were interpolated into 10-km gridded data (see Yang et al. (2004) for more details). The daily potential evaporation is estimated in each grid using the Penman equation recommended by Shuttleworth (1993). Finally, the daily potential evaporation was resampled to the same spatial resolution (0.25° × 0.25°) as with the precipitation.

The European Space Agency (ESA) climate change initiative (CCI) remotely sensed soil moisture product (http://www.esa-soilmoisture-cci.org/) was used to validate the identified drought events. This soil moisture product was merged from active and passive microwave satellite sensors, with daily temporal resolution and 0.25° spatial resolution, covering the period from November 1978 to December 2010 (Liu et al., 2012; Wagner et al., 2012).

For the convenience of analysis, mainland China was divided into three major regions: humid region, arid region and transition region (sub-humid and semi-arid region), with aridity indices ranging from 0–0.2, 0.2–0.75, >0.75, respectively, based on the classification of aridity index (UNESCO, 1979). The arid region was excluded for drought identification due to two reasons: (1) replenishment of water resources in the arid region is mainly from melted glacial or perennial frozen soil, and not from precipitation; and, (2) meteorological observations in this region are too scarce to conduct robust analysis (see Fig. 1).

2.2. Calculation of drought indices

(1) Potential evaporation

Drought indices used in the study are constructed based on precipitation and potential evaporation. Penman equation (Penman, 1948) is the common method to calculate E_p, which is more physically-based, incorporating humidity, air pressure, wind speed, and radiation. Thornthwaite equation (Thornthwaite, 1948) has been used for comparison.

a. Penman equation

Penman (1948) combined energy balance with mass transfer and derived an equation to calculate the evaporation from an open water surface from standard climatic condition. It can be written as (Shuttleworth, 1993):

$$E_p = E_{pR} + E_{pA} = \frac{\Delta}{\Delta+\gamma}R_n + \frac{\gamma}{\Delta+\gamma}\frac{6430(1+0.536u_2)D}{\lambda} \quad (1)$$

where E_p (mm day^{-1}) is the potential evaporation, E_{pR} (mm day^{-1}) is the radiative component, E_{pA} (mm day^{-1}) is the aerodynamic component, R_n (M J M^{-2} Day^{-1}) is daily net radiation, u_2 (m s^{-1}) is daily average wind speed at 2 m height, D (Pa) is the vapor pressure deficit, Δ (Pa K^{-1}) is the slope of the saturation vapor pressure vs. temperature curve, γ (Pa K^{-1}) is the psychrometric constant, γ (2.45×10^6 J kg^{-1}) is the latent heat of vaporization of water. R_n is the difference between the incoming net short wave radiation (R_{ns}) and the net outgoing long-wave radiation (R_{nl}), both in M J M^{-2} Day^{-1}:

$$R_n = R_{ns} - R_{nl} \quad (2)$$

with R_{ns} and R_{nl} being calculated by:

$$R_{ns} = (1-\alpha)R_s \quad (3)$$

$$R_{nl} = \frac{\sigma T_{\max}^4 + \sigma T_{\min}^4}{2}(0.34 - 0.14\sqrt{e_a})\left(\frac{1.35(a_s + b_s n/N)}{a_s + b_s} - 0.35\right) \quad (4)$$

where a_s is the faction of extraterrestrial radiation reaching the earth on overcast days, $a_s + b_s$ is the fraction extraterrestrial radiation reaching the earth on clear days. a_s and b_s are Ångström coefficients, which are derived from regression analysis of measurements of short wave radiation and sunshine hours from different meteorological stations in this study. α is albedo, n is observed sunshine hours, N is potential sunshine hours, σ ($4.903 * 10^9$ M J K^{-4} m^{-2} day^{-1}) is the Stefan–Boltzmann constant, $T_{\max}$ and $T_{\min}$ is the maximum and minimum absolute air temperature (K), R_s (M J M^{-2} Day^{-1}) is the global solar radiation, which can be calculated by the Ångström-Prescott formula (Martinez-Lozano et al., 1984):

$$R_s = \left(a_s + b_s\frac{n}{N}\right)R_a \quad (5)$$

where R_a (M J M^{-2} Day^{-1}) is the extra-terrestrial solar radiation.

In this study, the potential evaporation calculated by Penman equation is used to calculate the drought indices for investigating the spatio-temporal characteristics of droughts occurred in China during the past half century.

b. Thornthwaite equation

In many studies of droughts, Thornthwaite equation has been used to calculate the potential evaporation, denoted as E_p_th for distinguishing from the E_p calculated by Penman equation. E_p_th is calculated as:

$$E_p\_\text{th} = 16\left(\frac{N}{12}\right)\left(\frac{NDM}{30}\right)\left(\frac{10T}{H}\right)^m \quad (6)$$

where T is the monthly mean temperature (°C), N is the maximum number of sunshine hours, NDM is the number of days of the month, H is a heat index, which is calculated as the sum of 12 monthly indices,

$$H = \sum_{i=1}^{12}\left(\frac{T_i}{5}\right)^{1.514} \quad (7)$$

m is a coefficient depending on H, and which is defined as:

$$m = 6.75 \times 10^{-7}H^3 - 7.71 \times 10^{-5}H^2 + 1.79 \times 10^{-2}H + 0.492 \quad (8)$$

The potential evaporation calculated by Thornthwaite equation relies on the air temperature only. In this study it was used for comparison with the potential evaporation calculated by Penman equation for discussing the impact of global warming (temperature increasing) on drought.

(2) Standardized precipitation index (SPI)

The process of SPI calculation can be summarized into the follow steps (McKee et al., 1993): Firstly, choose the aggregation time step, denoted by *ts*. For the monthly precipitation time series of P_i ($i = 1, 2, \cdots, i, i+1, \cdots, n$), the *ts* months accumulated precipitation (P_sum_i) of the *i*th month ($i \geqslant ts$) is:

$$P\_sum_i = \sum_{j=i-ts+1}^{j=i} P_j \tag{9}$$

Secondly, fit an appropriate probability distributions to the time series *P_sum* of each month (from January to December). In this study, the most commonly used gamma distribution was selected. The probability density function $g(x)$ and cumulative distribution function $G(x)$ are listed below:

$$g(x) = \frac{1}{b^a \Gamma(\alpha)} x^{a-1} e^{-x/b}, \quad \text{for } x > 0 \tag{10}$$

$$G(x) = \frac{1}{b^a \Gamma(a)} \int_0^x t^{a-1} e^{-t/b} dt, \quad \text{for } x > 0 \tag{11}$$

$$H(x) = q + (1-q)G(x) \tag{12}$$

where x is *P_sum* in Eq. (9), a and b are the shape and scale parameters, respectively, estimated by the maximum likelihood method. Since precipitation is not continuous over time, Eq. (12) is used to account for such physical feature of precipitation, where q is the probability of zero. If m is the numbers of zeros, M is the length of the sequence, then q can be estimated as m/M. Finally, SPI value is obtained by transforming H to the standard normal distribution:

$$\mathrm{SPI} = \varphi^{-1}(H) \tag{13}$$

where φ is the standard normal distribution.

(3) Reconnaissance Drought Index (RDI)

The ratio P/E_p for a certain period would reflect the climatic moisture deficiency, thus a good indicator to construct drought index. Tsakiris et al. (2007) calculated the aggregated deficit (α) between cumulative precipitation and cumulative potential evaporation as:

$$\alpha_i = \frac{\sum_{j=i-ts+1}^{j=i} P_j}{\sum_{j=i-ts+1}^{j=i} E_{p_j}} \tag{14}$$

where *ts* is the aggregation time step, P_j is the precipitation of the *j* th month, E_{pj} is the potential evaporation of the *j* th month. The same procedures as those in the calculation of SPI were transplanted here to obtain RDI values, according to Eqs. (10), (11), (12), (13).

(4) Standardized Pricipitation Evapotranspiration Index (SPEI)

Vicente-Serrano et al. (2010) used the difference (Δ) of P and E_p instead of the quotient to measure the water surplus or deficit:

$$\Delta_i = P_i - E_{p_i} \tag{15}$$

Then, Δ is aggregated at *ts* as:

$$\Delta\_sum_i = \sum_{j=i-ts+1}^{j=i} \Delta_j \tag{16}$$

Three-parameter log–logistic distribution was suggested by Vicente-Serrano et al. (2010) to fit the twelve time series Δ_sum of each month (January to December). The probability density function $f(x)$ and cumulative distribution function $F(x)$ are listed below:

Table 1
Drought classifications based on SPI, RDI, and SPEI.

Drought class	Probability (%)	Index value
Extreme wet	2.3	$\geqslant 2.0$
Very wet	4.4	1.5∼2.0
Moderate wet	9.2	1.0∼1.5
Near normal	68.2	−1.0∼1.0
Moderate dry	9.2	−1.5∼−1.0
Severe dry	4.4	−2.0∼−1.5
Extreme dry	2.3	$\leqslant -2.0$

$$f(x) = \frac{\beta}{\alpha}\left(\frac{x-\gamma}{\alpha}\right)^{\beta-1}\left[1+\left(\frac{x-\gamma}{\alpha}\right)^{\beta}\right]^{-2} \tag{17}$$

$$F(x) = \left[1+\left(\frac{\alpha}{x-\gamma}\right)^{\beta}\right]^{-1} \tag{18}$$

where x is Δ_sum in Eq. (16), α, β and γ are scale, shape, and location parameters, respectively, which are obtained by the maximum likelihood method. Finally, the SPEI is calculated by transforming F to the standard normal distribution, following Eq. (13). The calculation of SPEI was carried out by the R package SPEIcalc (URL: http://sac.csic.es/spei) developed by Vicente-Serrano et al. (2010).

Since SPI, RDI and SPEI follow similar methodologies, their values should have the same statistical meaning, and therefore are comparable. Therefore, we used the same threshold for the three indices to classify the drought conditions (see Table 1).

2.3. Drought event identification and characterization

In the present study, SPI3, RDI3 and SPEI3 (time scale = 3 months) are selected, as they are capable of representing the seasonal droughts. A threshold value of −1 is selected to identify the drought condition. With the drought index calculated for each 0.25° × 0.25° grid from 1961 to 2012, drought events are extracted using a space–time continuum identification method proposed by Andreadis et al. (2005) and improved by Lloyd-Hughes (2012). The aim of this method is to identify coherent space and time structures in a 3-dimensional array (longitude, latitude, and time) of drought index, denoted by DI. The size of DI is $n_{\mathrm{lon}} \times n_{\mathrm{lat}} \times n_t$, where $n_{\mathrm{lon}}, n_{\mathrm{lat}}$ are numbers of girds along the longitude and latitude, respectively, and n_t is number of months along the time dimension. Then the following three steps are implemented to extract drought events.

Step 1: Identifying drought patches in the study area for each month. For the i th month, drought patches are extracted based on the clustering algorithm of Andreadis et al. (2005). A drought patch is a set of grids with the value of drought index less than −1 which are connected with each other. Repeat for 52 * 12 months and mark different patches with different labels. A label array L with the same size of DI is used to store the labels of each voxel.

Step 2: Determining the connection of drought patches on two adjacent months. Considering two adjacent months, namely, the *i* th and *i* – 1th, if any couples of patches (denoted by p_{i-1} and p_i) between the two months have an overlap area larger than a predetermined threshold, then the two patches belong to the same drought event.

Step 3: Identifying drought events during the study period. Searching from the first month to the $i-1$th month, all the patches which have the same label with p_{i-1} are updated to the label of p_i. This searching process is executed sequentially from the second month of the 52-years to the last month. Finally, all the drought events are identified as a series of drought patches in continuous

time and marked with different labels. A set of voxels in L with the same label belong to the same drought event.

The threshold area is the only parameter used in this clustering scheme. Sheffield et al. (2009) found that drought clusters with smaller area threshold could persist many years through tenuous spatial connectivity, and suggested a threshold of 500,000 km^2 for global drought analysis. Lloyd-Hughes (2012) used the same threshold of 500,000 km^2 in analyzing European drought over an area of 10 million km^2. Wang et al. (2011) examined the sensitivity of the drought identification results to the threshold area, and found that a threshold of 150,000 km^2 was the most suitable in China with an area of 9.6 million km^2. Since the non-arid region in China is about 6.6 million km^2 (about 2/3 of the total area of China), a threshold area of 100,000 km^2 (2/3 of the threshold area suggested by Wang et al. (2011)) was selected in this study.

Then five parameters are calculated to characterize the identified drought events. They are defined below:

(1) Duration (D) is the persistent time of a drought event, calculated as the time-span between the initiation time and the termination time of a drought event. In other words, it represents the time length of a drought event.

(2) Severity (S) is an expression of water shortage, indicating the total amount of water that is needed to recover back to normal condition. A drought event consists of a set of drought voxels with the same label. The severity of the drought event (taking the n^{th} as an example) is defined as:

$$S_n = \sum_{i=1}^{n_{lon}} \sum_{j=1}^{n_{lat}} \sum_{k=1}^{n_t} s(i,j,k) \tag{19}$$

$$s(i,j,k) = \begin{cases} DI(i,j,k) * area(i,j,k) * time(i,j,k), & L(i,j,k) = l_n \\ 0, & L(i,j,k) \neq l_n \end{cases} \tag{20}$$

where S_n is the severity of the n^{th} drought event (km^2 month), S is the severity of voxels (km^2 month), l_n is the label of the n^{th} drought event, *area* and *time* are the areas and heights of voxels, *time* is one month here since the monthly data is used.

(3) Affected Area (A) is the area swept by a drought event. It is the projected area over the longitude–latitude surface in the 3-dimensional space–time domain.

(4) Intensity (I) is introduced to discriminate between drought events with large volumes arising from long duration over a wide area and those accrued from short periods over limited area.

$$I = \frac{S}{D * A} \tag{21}$$

(5) Centroid (C) is the center of the drought event, representing the position (longitude, latitude, time) of the drought event in the 3-dimensional space–time domain. The MATLAB image processing function *regionprops* (MathWorks, 2014) was adopted to extract the centroids of drought events.

3. Results

A total of 958, 863 and 714 drought events were identified based on SPI3, RDI3, and SPEI3, respectively (hereafter referred to as SPI3 drought, RDI3 drought, and SPEI3 drought), over the non-arid zone of mainland China in the period from 1961 to 2012. Droughts which last for a longer time would be more hazardous, thus drought events lasting 3 months or longer are analyzed in this study. They respectively have 143, 149, and 176 events for SPI3, RDI3 and SPEI3. SPI3 has the minimum proportion (143 of 958) of long duration drought events, while SPEI3 has the maximum (176 of 714). This is because E_p exhibits smoother gradients of variability in both space and time than P, leading to the inference that RDI and SPEI voxels are more likely to be connected.

3.1. Validation of the identified drought events

Given that historical records of drought are very limited, it is difficult to evaluate the rationality of the identified drought events directly. Here we proposed an indirect cross validation using remotely sensed soil moisture data, since drought is the major cause of dryness of soil moisture. Soil moisture condition could reflect the degree of meteorological drought to some extent.

The ESA-CCI remotely sensed soil moisture product is firstly normalized to remove its seasonality, according to:

$$n\_SM = \frac{SM - \overline{SM}}{\sigma} \tag{22}$$

where SM is soil moisture series to be normalized, $\overline{SM}$ and σ are the mean and standard deviation of SM, and n_SM is the normalized soil moisture. This normalization was carried out on each grid for each month (from January to December). The corresponding n_SM cluster for each drought event identified by SPI3 (and RDI3, SPEI3) was extracted with the same spatial and temporal extent to ensure that they have the same duration and affected area. The severity of n_SM clusters were calculated by Eqs. (19) and (20).

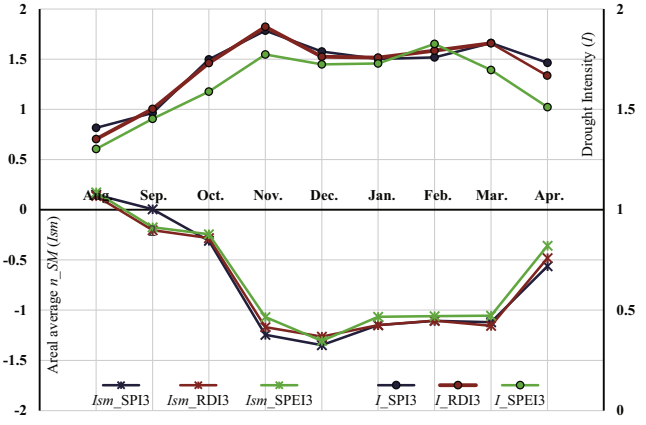

Fig. 2. Relationship between the SPI3, RDI3, SPEI3 drought intensity (I) and the areal average normalized soil moisture (Ism) during the southwest drought from August 2009 to April 2010 (n_SM: normalized soil moisture).

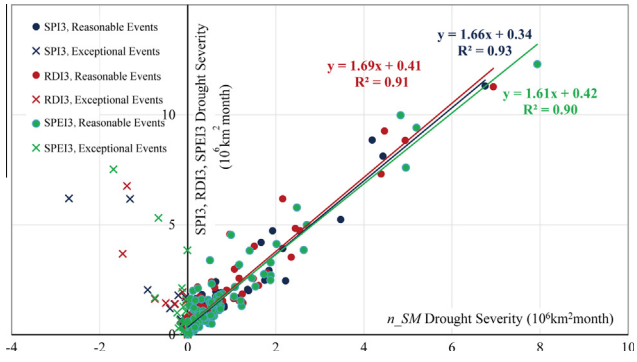

Fig. 3. Correlation between the drought severity based on the normalized soil moisture (n_SM) and SPI3, RDI3, SPEI3. (*Note*: Exceptional events in the left quadrant with negative n_SM drought severity mean that soil moisture is above normal condition during the meteorological drought period, which may be resulting from artificial irrigation especially in farmland, and/or from shallow groundwater, or due to errors in the remote sensing soil moisture data.)

Table 2
Top 10 drought events ranked by severity.

Drought index	Label	Rank	Persistent Period (yyyy.mm)	Duration (month)	Centroid (lon, lat, t) (E, N, yyyy.mm)	Affected area (10^6 km^2)	Severity (10^6 km^2 month)	Intensity
SPI3	*a*	1	2010.12–2011.11	12	111.09, 29.81, 2011.05	3.15	19.28	0.51
	b	2	1998.10–1999.03	6	111.75, 33.59, 1999.01	2.76	13.58	0.82
	c	3	1963.01–1963.09	9	113.77, 26.27, 1963.05	1.45	10.36	0.79
	d	4	1962.02–1962.07	6	109.66, 33.38, 1962.04	2.86	9.76	0.57
	e	5	2009.08–2010.04	9	105.84, 26.25, 2009.12	1.74	9.24	0.59
	f	6	1968.12–1969.06	7	99.61, 28.87, 1969.03	1.86	9.06	0.69
	g	7	1965.01–1961.11	11	114.34, 40.24, 1965.06	1.50	8.64	0.53
	h	8	1997.06–1997.12	7	109.48, 34.13, 1997.09	1.60	8.59	0.77
	i	9	1984.01–1984.05	5	112.74, 31.70, 1984.03	2.36	8.01	0.68
	j	10	2001.04–2001.11	8	113.96, 33.27, 2001.08	1.63	7.47	0.57
RDI3	*c*	1	1962.10–1963.10	13	111.84, 30.67, 1963.03	4.51	24.33	0.42
	a	2	2010.12–2011.10	11	111.68, 29.98, 2011.04	3.04	16.80	0.50
	b	3	1998.10–1999.04	7	111.67, 33.79, 1999.01	2.86	13.63	0.68
	f	4	1968.12–1969.07	7	100.53, 28.79, 1969.03	2.00	11.19	0.80
	d	5	1962.02–1962.07	6	110.74, 33.05, 1962.04	2.87	10.93	0.64
	g	6	1965.01–1965.11	11	115.55, 41.14, 1965.07	1.85	10.54	0.52
	e	7	2009.08–2010.04	9	105.73, 26.04, 2009.12	1.64	9.62	0.65
	h	8	1997.06–1997.12	7	109.78, 34.40, 1997.09	1.75	9.27	0.76
	–	9	1995.03–1995.08	6	103.78, 35.23, 1995.05	1.98	8.18	0.69
	–	10	1979.10–1980.01	4	112.48, 29.54, 1979.12	2.46	7.76	0.79
SPEI3	*c*	1	1962.10–1963.10	13	114.80, 34.33, 1963.04	4.77	31.68	0.51
	–	2	1965.05–1966.07	15	114.52, 39.14, 1965.12	2.30	17.95	0.52
	f	3	1968.12–1969.07	8	101.01, 29.76, 1969.03	2.38	16.60	0.87
	b	4	1998.09–1999.04	8	111.01, 31.55, 1999.01	3.24	16.48	0.64
	–	5	1966.06–1967.04	11	116.92, 36.41, 1966.11	3.49	16.37	0.43
	–	6	1972.05–1972.12	8	112.74, 39.30, 1972.09	2.74	16.20	0.74
	a	7	2010.12–2011.10	11	111.63, 29.73, 2011.4	2.91	15.58	0.49
	d	8	1962.02–1962.07	6	111.69, 32.90, 1962.04	2.85	12.01	0.70
	e	9	2009.08–2010.04	9	105.24, 26.11, 2009.12	1.77	10.44	0.66
	–	10	1968.02–1968.09	8	115.73, 35.88, 1968.05	2.00	10.29	0.64

Note: "–" means that there's no corresponding drought event in this table.

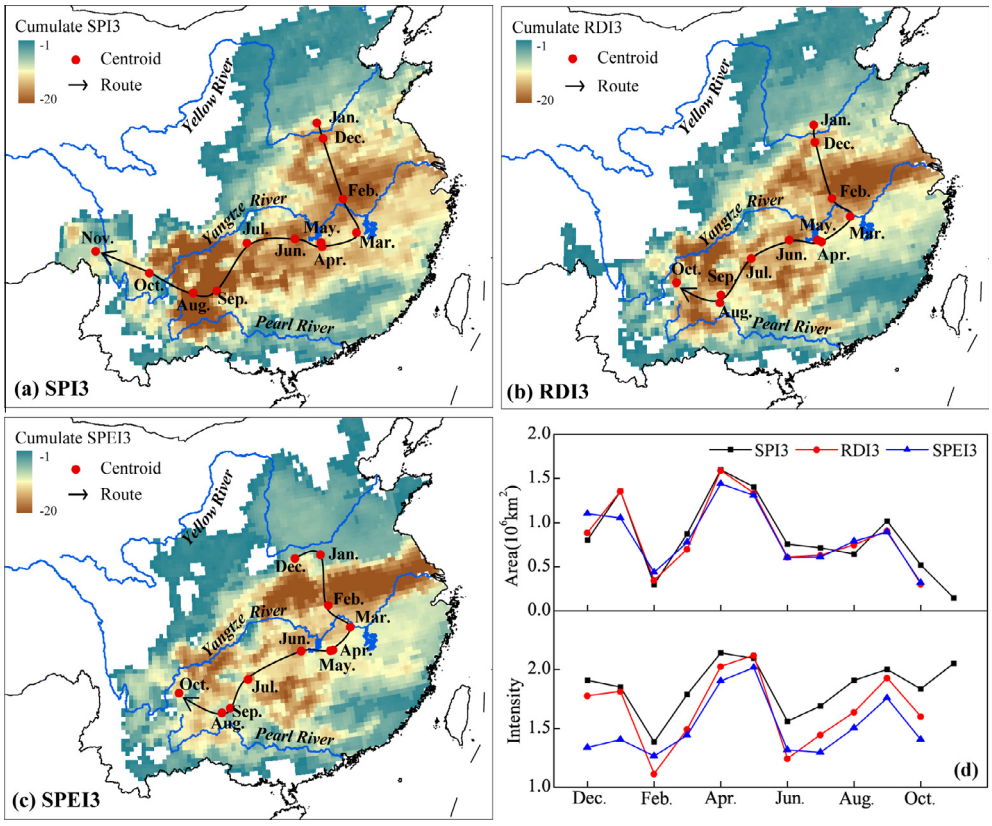

Fig. 4. Typical drought development process from December 2010 to November 2011.

The most severe drought event occurred in 1979–2010 is selected for validation based on the available soil moisture data. This drought lasted 9 months, from August 2009 to April 2010, affecting an area of 1.7 million km^2 in southwest China. It was reported to be the most severe drought during the past half-century in this region (Yang et al., 2011), causing great damage to the local eco-environment and socio-economy (Zhang et al., 2012a). Fig. 2 shows the changes of the SPI3, RDI3, and SPEI3 drought intensity and the corresponding areal averaged normalized soil moisture. It indicates that the drought index has the opposite changing pattern with the soil moisture. Taking SPI3 as an example, during the drought developing stage (from August 2009 to November 2009), the drought was intensified rapidly (I increase from 1.41 to 1.89) while the soil moisture decreased from the near normal condition ($n\_SM = 0.15$) to a deficit level ($n\_SM = -1.35$). This water deficit continued for another four months (from November 2009 to March 2010), with the n_SM staying below −1. Finally, the diminished stage (from March 2010 to April 2010) witnessed a decrease of drought intensity (from 1.83 to 1.73), coinciding with the increase of soil moisture (n_SM increased from −1.12 to −0.56). Obviously, the variation of remotely sensed soil moisture was consistent with the variation of identified drought event along the time dimension. It also shows that the RDI3 and SPEI3 have similar patterns, implying that the drought events identified by the three indices are reasonable.

Fig. 3 plots the n_SM drought severity (x-axis) vs. SPI3, RDI3, and SPEI3 drought severity (y-axis). According to SPI3, 93 drought events (90 and 103 for RDI3 and SPEI3) in total are identified with durations equal to or longer than 3 months during the period from 1979 to 2010. Clearly, for most of the identified drought events, the SPI3 drought severity and the n_SM drought severity correlate well (see the right quadrant in Fig. 3), with the coefficient of determination (R^2) of 0.93 (0.91 and 0.90 for RDI3 and SPEI3). However, there are 15 outliers for the SPI3 drought events (12 and 18 for RDI3 and SPEI3), in which the surface soil moisture content (indicated by the negative value of n_SM drought severity) were above the normal condition (see the left quadrant in Fig. 3). This means wet conditions according to the remotely sensed soil moisture data. The reason for such conditions (negative values of n_SM drought severity) identified by the soil moisture may be due to the impact of artificial irrigation especially in the farmland, and/or impact of shallow groundwater, or it may be due to errors in the remotely sensed soil moisture data. Apart from these limited numbers of negative values of n_SM drought severity, most of the drought events detected by the indices of SPI3, RDI3 and SPEI3 can be validated by the remotely sensed soil moisture data.

3.2. Major drought events identified in the past 52 years

The top 10 drought events ranked by their severities are listed in Table 2. The most severe SPI3 drought (December 2010 to November 2011) swept from the North China Plain to the middle reach of Yangtze River, and diminished eventually in southwest China, covering about 3.15 million km^2. It ranks as the second and seventh in the list of drought events by RDI3 and SPEI3, respectively. The most severe RDI3 and SPEI3 drought lasted from October 1962 to October 1963, starting from both Haihe River basin in the north and Pearl River basin in the south, and ending in southeastern China with a coverage of 4.5 million km^2. It ranks as the third in the SPI3 droughts. To check with the similarity among the different indices, we used the same labels (from a to j) to mark the drought events, indicating that the events occurred approximately in the same period and in the same region. As Table 2 shows there are 8 drought events with the same label for SPI3 and RDI3, and 6 events for SPI3 and SPEI3 (for RDI3 and SPEI3). This suggests that the results based on SPI3 and RDI3 would be more likely to have similar behavior compared to that of SPI3 and SPEI3.

Fig. 4 illustrates the spatio-temporal developing process of the 2011 drought based on SPI3 (Fig. 4a), RDI3 (Fig. 4b) and SPEI3 (Fig. 4c). The stretched color maps show the spatial distribution

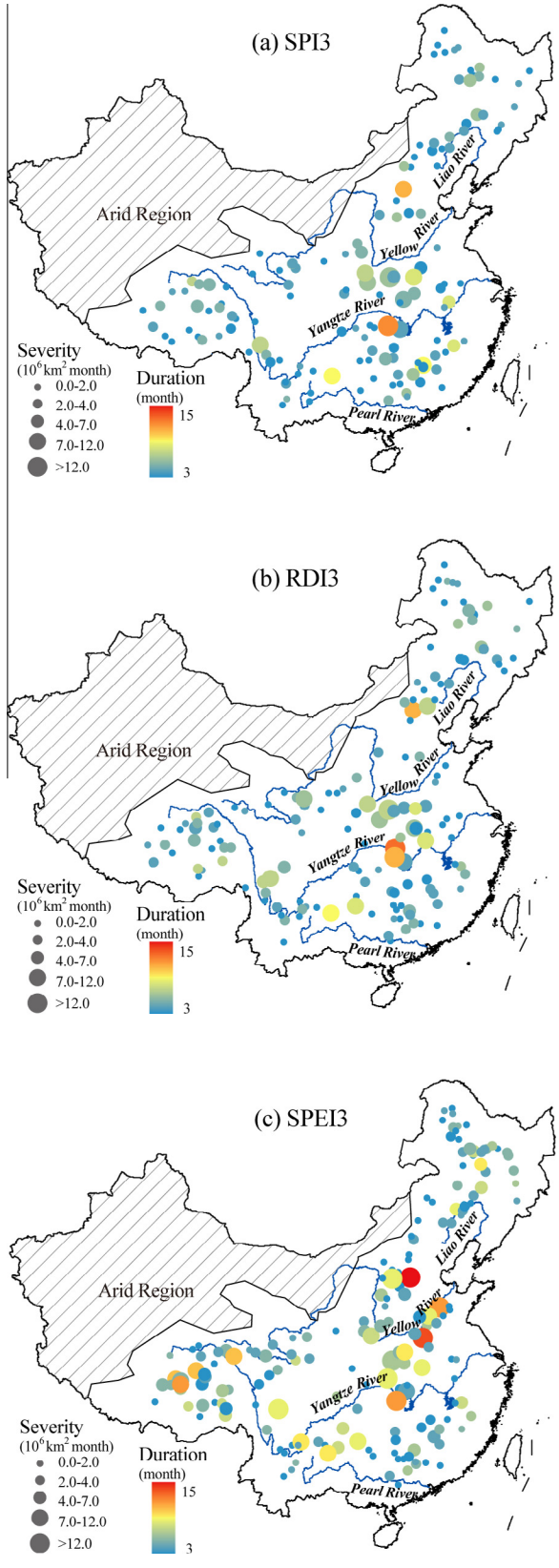

Fig. 5. Spatial distribution of drought events during 1961–2012.

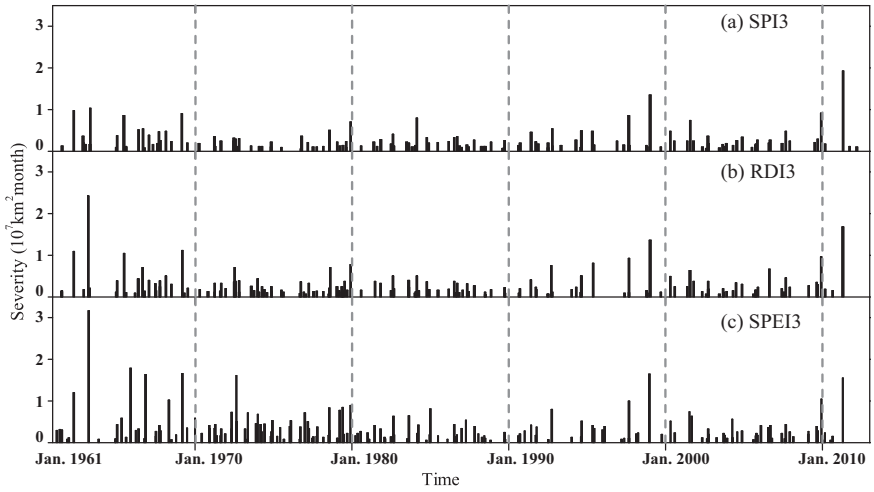

Fig. 6. Temporal variation of drought severity during 1961–2012.

of the cumulative value of the drought index throughout the lifetime of the event. The red dots are the centroids of the drought patches for each month, between which the black arrows express the moving paths of the drought. Variability of the areal extent and intensity in this drought are compared in Fig. 4d. The spatial and temporal variations of this drought identified by the three indices are almost the same except for the duration. Drought shown in Fig. 4a lasted one month longer and is more severe than the ones given in Fig. 4b and c. This drought originated from the southern part of North China Plain, and shrank to the middle and lower reach of the Yangtze River in February 2011 with the area decreased by 70%, and the intensity decreased by 20% (Fig. 4d). It persisted around the Poyang and Dongting Lakes from February to June 2011 with an increasing intensity and severity, causing drying up of these two largest fresh water lake in China (Sun and Yang, 2012; Jin et al., 2013). It moved along the Yangtze River to the Yunnan-Guizhou Plateau from June to September 2011, and finally diminished in the Hengduan Mountains. This drought consists of three sub-droughts, North China Plain drought (December to February), Poyang and Dongting Lake drought (February to June), Yunnan-Guizhou Plateau drought (June to October).

3.3. The spatial and temporal variation of drought events

The three indices showed fairly consistent results in capturing the large magnitude drought events as discussed in Sections 3.1 and 3.2. In this section, the spatial and temporal variations of drought events during 1961–2012 are analyzed.

Fig. 5 plots the spatial distribution of each drought centroid with circles of different colors representing durations as well as various sizes representing severities. Fig. 5a shows that SPI3 droughts with long duration and great severity mainly cluster over the area between the downstream of Yellow River and the downstream of Yangtze River. The spatial distribution of RDI3 drought events is almost the same as with SPI3 (Fig. 5b). However, the results of SPEI3 (Fig. 5c) are quite different from those of SPI3 and RDI3. It shows a noticeable shift of the locations of large magnitude SPEI3 droughts, which concentrates in the North China Plain. This result is consistent with the analysis by China Meteorological Agency (CMA) based on CI (CMA, 2007). It is consistent with the results of the three indices (Fig. 5a–c) that droughts in northeast and southeast China are usually with short durations and small severities.

Fig. 6 illustrates the temporal variation of droughts in the non-arid region of mainland China. Severities are used to express the magnitude of droughts and they are located based on their centroid

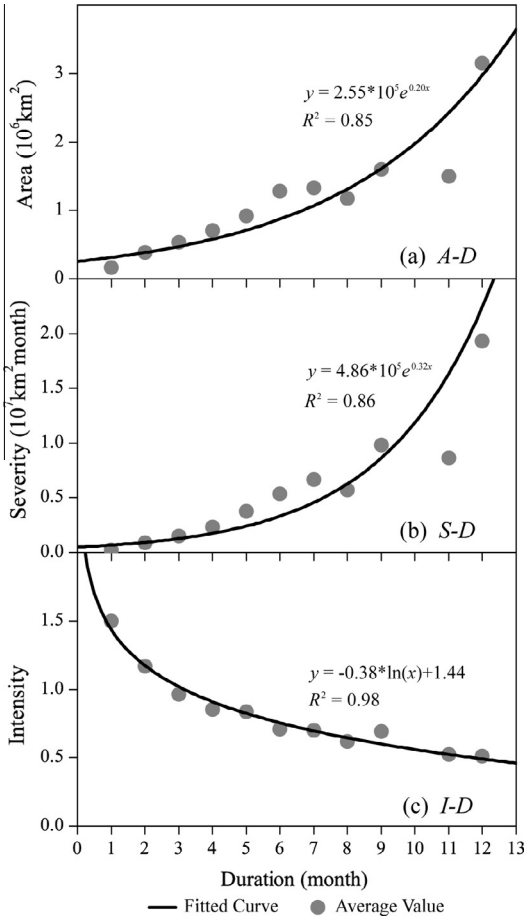

Fig. 7. Changes of drought affected area (a), severity (b), and intensity (c) with duration.

coordinates along the time dimension. It shows that drought occurrence in the 1960s is more serious than in other decades. The temporal variations of droughts after 1980 show satisfactory consistency among the three indices, with drought severity showing a non-significant increasing trend ($\alpha = 0.05$) by the Mann–Kendall trend test (Kendall, 1948). Two large magnitude droughts occurred after 2010, and they have been analyzed in Sections 3.1 and 3.2. The drought temporal variations identified by the three

indices are quite different before 1980. It shows that SPI3 drought severities are much smaller than those of RDI3 and SPEI3, and the number of SPI3 drought events is much less than those of RDI3 and SPEI3 in the 1960s and 1970s (a total of 53, 67, 77 drought events are identified in this period based on SPI3, RDI3, and SPEI3 respectively). Also, from Figs. 5 and 6 it is seen that large magnitude SPEI3 droughts over the North China Plain, the Yunnan-Guizhou Plateau, and the Tibetan Plateau occurred mainly in the 1960s and 1970s. The discrepancies of SPI3, RDI3 and SPEI3 before 1980 are the main sources of the differences of the drought spatial and temporal variation patterns in Figs. 5 and 6.

4. Discussion

4.1. Changes of drought affected area, severity, intensity with duration

The average values of affected area, severity and intensity for different drought durations are used to explore the variation of drought magnitude with duration. Fig. 7 shows the relationships of affected area (A), severity (S), intensity (I) with duration (D) based on the SPI3 index. The drought affected area and drought severity show exponential changes with duration, as indicated by the fitted exponential functions to the A–D and S–D curves which have coefficients of determination (R^2) of 0.85 and 0.86, respectively. A log function was used to fit to the I–D cure, with $R^2 = 0.98$. Similar relationships were also found based on RDI3 and SPEI3 indices, with R^2 values of A–D, S–D, and I–D curves all above 0.85. This means the magnitude of drought may increase exponentially with the duration. These relationships would also be useful for drought frequency analysis and drought impact assessment. Given that drought events with duration more than 10 months are scarce, there would exist uncertainties in these curves, particularly in the upper tails. To reduce such uncertainties, paleo-drought reconstructions and Monte Carlo simulations would be helpful. Yet this is not in the scope of the present study.

4.2. Drought trends influenced by precipitation and potential evaporation

Climate change has been recognized as one of the major threats to the earth environment in the 21st century (IPCC, 2007; Mishra and Singh, 2010), and it has profound impacts on drought by changing the climatic water supply (P) and/or water demand (E_p). Mann–Kendall (MK) trend test (Kendall, 1948) on SPI3, RDI3, SPEI3, P and E_p were carried out, in order to evaluate the changes of drought and the possible causes. Monthly P and E_p were firstly normalized (denoted by n_P and n_E_p, respectively) according to Eq. (22) before the MK test and trend analysis, in order to remove their seasonality.

Fig. 8 shows the results of MK trend analysis using the significance level of $\alpha = 0.05$. The stretched color map is the MK trend (10^{-3} per month). Regions marked with red dots are significantly drying areas, and regions marked with black dots are significantly wetting areas. There is a significant wetting trend over Tibetan Plateau, which is mainly caused by the increasing P and decreasing E_p. The western part of North China Plain, Loess Plateau, Sichuan Basin and Yunnan-Guizhou Plateau show significant drying trends, which is mainly caused by the dramatic decreasing of P, despite a significant decreasing trend of E_p. The northeast China and North China Plain show ambiguous drying and wetting patterns. The SPI3 shows an insignificant drying trend over most of this region, except for the far northern part of China which is significantly wetting (Fig. 8a). The SPEI3 shows that most regions are getting wetter (Fig. 8c), which is dominated by the significant decreasing trend of E_p (Fig. 8e).

Fig. 9 shows the MK trend of the normalized monthly temperature (Fig. 9a), the normalized monthly potential evaporation calculated by the Thornthwaite equation (Fig. 9b), the E_p_th based drought indices RDI3_th (Fig. 9c) and SPEI3_th (Fig. 9d). It is clear that the rapidly increasing temperature over most part of the study area shown in Fig. 9a caused the increasing trend of E_p_th shown in Fig. 9b, resulting in the significant drying trend shown in Fig. 9c

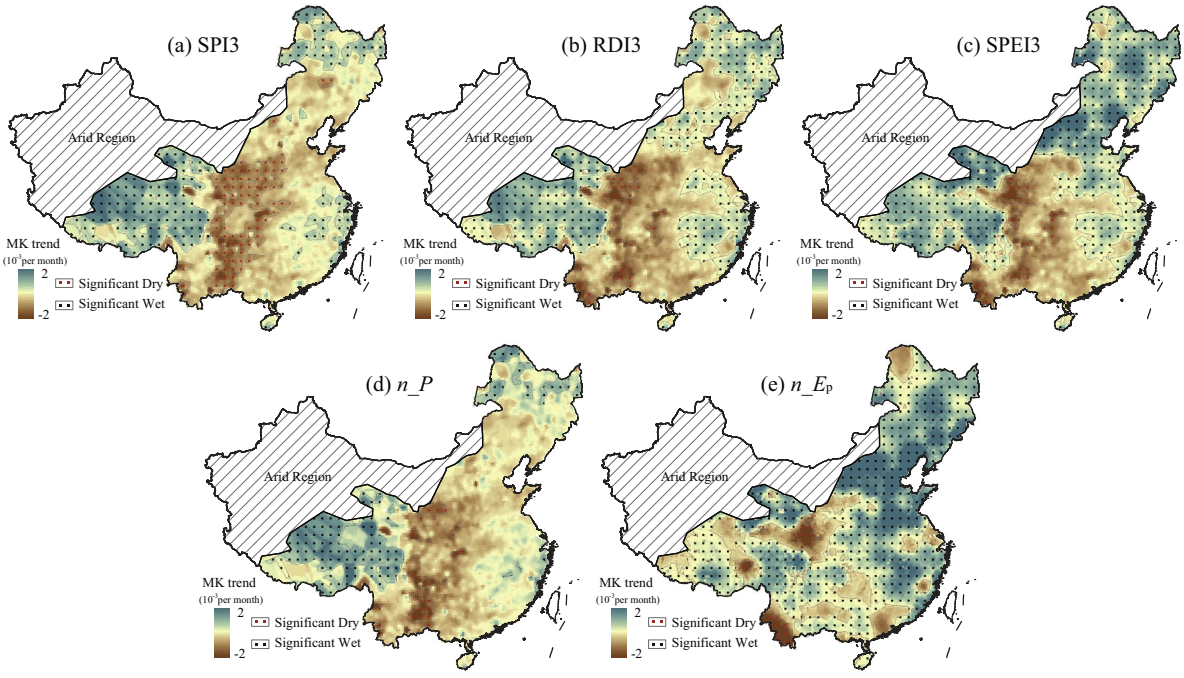

Fig. 8. Results of Mann–Kendall trend test of drought indices: (a) SPI3, (b) RDI3, and (c) SPEI3, and climatic index: (d) normalized monthly precipitation (n_P) and (e) normalized monthly Penman potential evaporation (n_E_p).

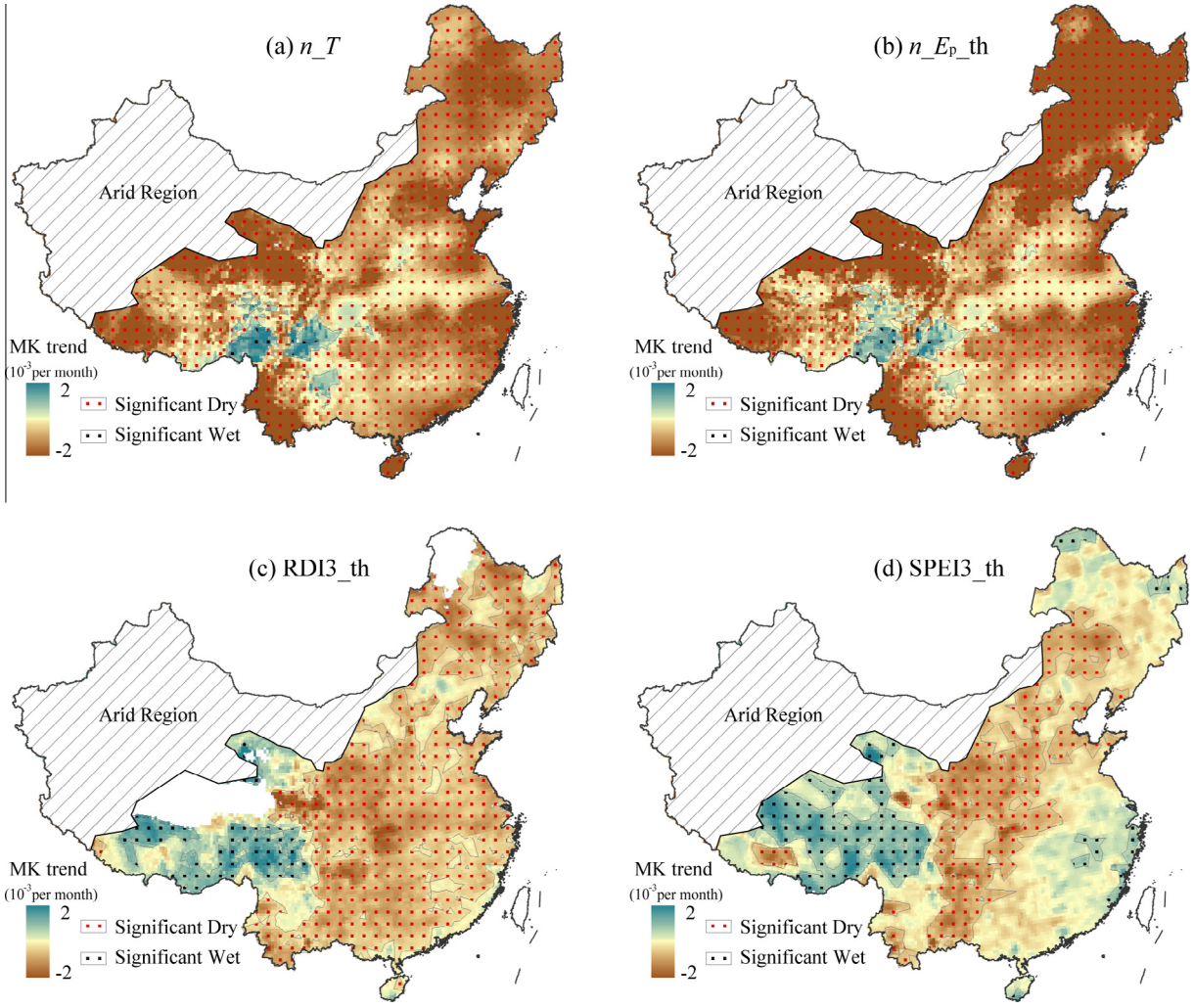

Fig. 9. Results of Mann–Kendall trend test: (a) normalized monthly temperature (*n_T*), (b) normalized monthly Thornthwaite potential evaporation (*n_Ep_*th), (c) RDI3 based on Thornthwaite potential evaporation, (d) SPEI3 based on Thornthwaite potential evaporation (SPEI3_th).

and d. Comparing Fig. 9c with Fig. 8e, we can see the distinct difference between the E_p_th trend and E_p trend, particularly in northern China. The decreasing trend of net radiation R_n (Gao et al., 2013; Tang et al., 2013) caused the decreasing trend E_p shown in Fig. 8e. Comparing Fig. 8b and c with Fig. 9c and d, we can conclude that the use of the potential evaporation calculated by Thornthwaite equation would exaggerate the drying trend during 1961–2012 in the mainland China because the Thornthwaite equation overestimates the temperature impact. Similarly, other researchers also pointed out the E_p_th based PDSI would exaggerate the drying trend in the global drought assessment (Sheffield et al., 2012; Dai, 2013).

4.3. Disadvantages of the climatic drought indices

Essentially, SPI, RDI, and SPEI are defined and calculated based on similar methodologies, and their values have the same statistical meaning. They share some common merits: (1) straightforward calculation procedures, (2) flexible time scales, (3) comparability through space and time. The major difference among the three indices is the meteorological variables used to construct the indices, *i.e.* P, P/E_p, and $P-E_p$, respectively. P/E_p and $P-E_p$ are different forms to represent the water sufficiency and deficiency. SPI only considers climatic water supply, while RDI and SPEI are formulated by taking both aspects of climatic water supply and demand. From this point, RDI and SPEI are better than SPI. The quotient form (P/E_p) of RDI restricts it application when E_p approaches zero such as in cold regions or in cold season, and makes RDI sensitive to changes of both P and E_p. The difference form ($P-E_p$) of SPEI has distinct behavior in relatively arid zones and relatively humid zones. In the relatively arid zones, E_p is usually much larger than P. Change of $P-E_p$ is mainly determined by E_p, therefore SPEI is E_p dominated. On the contrary, in the relatively humid zones P is usually larger than E_p and the change of SPEI is dominated by the change of P. As shown in Fig. 8, decreasing trend of SPEI3 is dominated by the decreasing trend of P (see Fig. 8c and d) in the relatively humid southern China though there is significant decreasing trend of E_p (see Fig. 8e). In contrast, the increasing trend of SPEI3 is dominated by the decreasing trend of E_p in the relatively arid Northeast China (see Fig. 8c and e) though there is decreasing trend of P (see Fig. 8d).

From the perspective of regional water budget, the total available water (water availability) for a region is actually as $P-ET$ (ET is the actual evaporation) rather than P/E_p or $P-E_p$. Therefore, the three indices are insufficient to reflect the deficit of water available. In the relatively humid regions, the performances of SPI, RDI, and SPEI are similar in capturing the drought condition (see Fig. 8a–c), because they are all dominated by P. In the relatively arid regions, ET is controlled by the precipitation (P), and the water availability ($P-ET$) is dominated by P. Therefore, SPI and RDI would perform better than SPEI in the relatively arid regions. Furthermore, RDI and SPEI are sensitive to potential evaporation (E_p).

Therefore, accurate estimation of E_p is important for drought assessment based on the indices of RDI and SPEI (see Fig. 9).

5. Conclusions

In this paper, a 3-dimensional clustering algorithm was used to identify drought events based on indices of SPI3, RDI3, and SPEI3 from 1961 to 2012 over non-arid regions of mainland China. Five drought characteristic parameters (duration, affected area, severity, intensity and centroid) were calculated to analyze the spatio-temporal variations of droughts. From the results presented in this study, the following conclusions can be made:

(1) The 3-dimensional drought identification method can capture the space–time structure of drought events effectively, and the five parameters are informative to analyze the spatio-temporal characteristics of droughts.
(2) There were 143, 149, 176 drought events with durations 3 months or longer from 1961 to 2012, identified on the basis of SPI3, RDI3, and SPEI3 respectively. The most severe SPI3 drought (from December 2010 to November 2011) swept from the North China Plain to the middle reach of Yangtze River, and diminished eventually in southwest China, covering about 3.15 million km^2. The most severe RDI3 and SPEI3 drought (from October 1962 to October 1963), started from both Haihe Basin in the north and Pearl River basin in the south, and ended in southeastern China with a coverage about 4.5 million km^2.
(3) The 1960s suffered the most serious drought occurrences during 1961–2012. The drought center where lots of large magnitude droughts were clustered stretches from North China Plain to the downstream of Yangtze River Basin. The western part of North China Plain, Loess Plateau, Sichuan Basin and Yunnan-Guizhou Plateau, show significant drying trends, which is mainly caused by the decreasing precipitation.
(4) Spatial and temporal variations of drought based on SPI3, RDI3, and SPEI3 show satisfactory consistent patterns after 1980, while inconsistent before 1980. This inconsistency is mainly caused by the decreasing trend of potential evaporation estimated by Penman equation over a large area of the non-arid zone in China. RDI and SPEI based on the potential evaporation estimated by the Thornthwaite equation tend to exaggerate the drought condition because the Thornthwaite equation overestimates the impact of air temperature.
(5) SPI, RDI, and SPEI perform almost the same in the relatively humid regions, but SPI and RDI are more suitable than SPEI in the relatively arid regions. RDI and SPEI are sensitive to the trend of E_p.

However, few limitations remain in the current study. The surface albedo α in Eq. (6) is variable with climate change or anthropogenic induced soil moisture and vegetation change (Zhang et al., 2012c), but was considered as a constant in calculating potential evaporation (E_p) in the present study. The bias of E_p due to this assumption may affect the reliability of RDI and SPEI. Also, the limited length of study period makes it impossible to distinguish the low frequency natural variability from drought spells. It is also necessary to point out that SPI, RDI, and SPEI cannot reflect the variation of water availability, which is of great concern to water resources management, particularly during the drought episode.

Acknowledgments

This research was supported by the National Natural Science Funds for Distinguished Young Scholar (Project No. 51025931) and National Natural Science Foundation of China (Project No. 51139002).

References

Andreadis, K.M., Clark, E.A., Wood, A.W., Hamlet, A.F., Lettenmaier, D.P., 2005. Twentieth-century drought in the conterminous United States. J. Hydrometeorol. 6 (6), 985–1001.
Bryant, E.A., 2005. Natural Hazards. University, Cambridge, UK, Cambridge.
Chen, Z., Yang, G., 2012. Analysis of drought hazards in North China: distribution and interpretation. Nat. Hazards 65 (1), 279–294.
CMA, 2006. Classification of Meteorological Drought. GB/T 20481-2006. China Meteorological Press, Beijing, China (In Chinese).
CMA, 2007. Altas of China Disastrous Weather and Climate China Meteorological Press, Beijing, China (In Chinese).
Dai, A., 2011. Drought under global warming: a review. Wiley Interdisciplinary Rev.: Clim. Change 2 (1), 45–65.
Dai, A.G., 2013. Increasing drought under global warming in observations and models. Nat. Clim. Change 3 (1), 52–58.
Dracup, J.A., Lee, K.S., Paulson, E.G., 1980. On the definition of droughts. Water Resour. Res. 16 (2), 297–302.
Gao, Y., He, H., Zhang, L., Lu, Q., Yu, G., Zhang, Z., 2013. Spatio-temporal variation characteristics of surface net radiation in China over the past 50 years. J. Geo-Inform. Sci. 1, 002.
Gocic, M., Trajkovic, S., 2014. Spatiotemporal characteristics of drought in Serbia. J. Hydrol. 510, 110–123.
Guttman, N.B., 1998. Comparing the Palmer drought index and the standardized precipitation index. JAWRA J. Am. Water Resources Assoc. 34 (1), 113–121.
Hao, Z., AghaKouchak, A., 2013. Multivariate standardized drought index: a parametric multi-index model. Adv. Water Resour. 57, 12–18.
He, B., Lü, A., Wu, J., Zhao, L., Liu, M., 2011. Drought hazard assessment and spatial characteristics analysis in China. J. Geogr. Sci. 21 (2), 235–249.
IPCC, 2007. Climate Change 2007 – The Physical Science Basis: Working Group I Contribution to the Fourth Assessment Report of the IPCC. Cambridge University Press.
Jin, D., Guan, Z., Tang, W., 2013. The Extreme Drought Event during Winter–Spring of 2011 in East China: Combined Influences of Teleconnection in Midhigh Latitudes and Thermal Forcing in Maritime Continent Region. J. Climate 26 (20), 8210–8222.
Kao, S.C., Govindaraju, R.S., 2010. A copula-based joint deficit index for droughts. J. Hydrol. 380 (1–2), 121–134.
Kendall, M.G., 1948. Rank Correlation Methods.
Khalili, D., Farnoud, T., Jamshidi, H., Kamgar-Haghighi, A.A., Zand-Parsa, S., 2011. Comparability analyses of the SPI and RDI meteorological drought indices in different climatic zones. Water Resour. Manage. 25 (6), 1737–1757.
Kim, S., Kim, B., Ahn, T.J., Kim, H.S., 2011. Spatio-temporal characterization of Korean drought using severity – area – duration curve analysis. Water Environ. J. 25 (1), 22–30.
Liu, Y.Y., Dorigo, W.A., Parinussa, R.M., de Jue, R.A., Wagner, W., McCabe, M.F., Evans, J.P., van Dijk, A.I.J.M., 2012. Trend-preserving blending of passive and active microwave soil moisture retrievals. Remote Sens. Environ. 123, 280–297.
Lloyd-Hughes, B., 2012. A spatio-temporal structure-based approach to drought characterisation. Int. J. Climatol. 32 (3), 406–418.
Lu, E., Luo, Y., Zhang, R., Wu, Q., Liu, L., 2011. Regional atmospheric anomalies responsible for the 2009–2010 severe drought in China. J. Geophys. Res. 116 (D21).
Lu, E., Cai, W., Jiang, Z., Zhang, Q., Zhang, C., Higgins, R.W., Halpert, M.S., 2013. The day-to-day monitoring of the 2011 severe drought in China. Clim. Dynam.
Ma, M., Ren, L., Yuan, F., Jiang, S.Y., Liu, Y., Kong, H., Gong, L., 2013. A new standardized Palmer drought index for hydro-meteorological use. Hydrol. Process., 10.
Martinez-Lozano, J., Tena, F., Onrubia, J., De La Rubia, J., 1984. The historical evolution of the Ångström formula and its modifications: review and bibliography. Agric. For. Meteorol. 33 (2), 109–128.
MathWorks, T., 2014. Image Processing ToolboxTM User's Guide, Version R2014a. The MathWorks.
McKee, T.B., Doesken, N.J., Kleist, J., 1993. The relationship of drought frequency and duration t time scales. In: Eighth Conference on Applied Climatology. American Meteorological Society, Anaheim, California.
Min, S.K., Kwon, W.T., Park, E.H., Choi, Y., 2003. Spatial and temporal comparisons of droughts over Korea with East Asia. Int. J. Climatol. 23 (2), 223–233.
Mishra, A.K., Singh, V.P., 2010. A review of drought concepts. J. Hydrol. 391 (1–2), 204–216.
Penman, H.L., 1948. Natural evaporation from open water, bare soil and grass. In: Proceedings of the Rolyal Society of London, Series A, Mathematical and Physical Sciences. The Rolyal Society, London, pp. 120–145.
Palmer, W.C., 1965. Meteorologic drought, US Department of Commerce, Weather Bureau, Research Paper No. 45.
Qian, W., Shan, X., Zhu, Y., 2011. Ranking regional drought events in China for 1960–2009. Adv. Atmos. Sci. 28 (2), 310–321.
She, D., Xia, J., 2012. The spatial and temporal analysis of dry spells in the Yellow River basin, China. Stoch. Environ. Res. Risk A 27 (1), 29–42.
Sheffield, J., Andreadis, K.M., Wood, E.F., Lettenmaier, D.P., 2009. Global and continental drought in the second half of the twentieth century: severity-area-

duration analysis and temporal variability of large-scale events. J. Clim. 22 (8), 1962–1981.
Sheffield, J., Wood, E.F., Roderick, M.L., 2012. Little change in global drought over the past 60 years. Nature 491 (7424), 435–440.
Shen, Y., Feng, M.N., Zhang, H.Z., Gao, F., 2010. Interpolation methods of China Daily Precipitation Data. J. Appl. Meteorol. Sci. 21 (3), 279–286 (In Chinese).
Shuttleworth, W.J., 1993. Evaporation. In: Maidment, D.R. (Ed.), Handbook of Hydrology. McGraw-Hill, New York.
Song, X., Li, L., Fu, G., Li, J., Zhang, A., Liu, W., Zhang, K., 2013. Spatial–temporal variations of spring drought based on spring-composite index values for the Songnen Plain, Northeast China. Theor. App. Climatol., 1–14.
Sun, C., Yang, S., 2012. Persistent severe drought in southern China during winter–spring 2011: large-scale circulation patterns and possible impacting factors. J. Geophys. Res. 117 (D10).
Tang, Y., Tang, Q., Tian, F., Zhang, Z., Liu, G., 2013. Responses of natural runoff to recent climatic changes in the Yellow River basin, China. Hydrol. Earth Syst. Sci. Discuss. 10 (4), 4489–4514.
Taylor, C.M., de Jeu, R.A., Guichard, F., Harris, P.P., Dorigo, W.A., 2012. Afternoon rain more likely over drier soils. Nature 489 (7416), 423–426.
Teuling, A.J., van Loon, A.F., Seneviratne, S.I., Lehner, I., Aubinet, M., Heinesch, B., Bernhofer, C., Grunwald, T., Prasse, H., Spank, U., 2013. Evapotranspiration amplifies European summer drought. Geophys. Res. Lett. 40 (10), 2071–2075.
Thornthwaite, C.W., 1948. An approach toward a rational classification of climate. Geogr. Rev. 38 (1), 55–94.
Tsakiris, G., Pangalou, D., Vangelis, H., 2007. Regional drought assessment based on the Reconnaissance Drought Index (RDI). Water Resour. Manage. 21 (5), 821–833.
UNESCO, 1979. Map of the World Distribution of Arid Regions: Explanatory Note. UNESCO.
Vicente-Serrano, S.M., Begueria, S., Lopez-Moreno, J.I., 2010. A multiscalar drought index sensitive to global warming: the standardized precipitation evapotranspiration index. J. Climate 23 (7), 1696–1718.
Vicente-Serrano, S.M., Begueria, S., Lorenzo-Lacruz, J., Camarero, J.J., Lopez-Moreno, J.I., Azorin-Molina, C., Revuelto, J., Moran-Tejeda, E., Sanchez-Lorenzo, A., 2012. Performance of drought indices for ecological, agricultural, and hydrological applications. Earth Interactions 16 (10), 1–27.
Wagner, M., Dorigo, W., de Jue, R., Fernandez, D., Benveniste, J., Haas, E., Ertl, M., 2012. Fusion of Active and Passive Microwave Observations to Create an Essential Climate Variable data Record on Soil Moisture, ISPRS Annals of the Photogrammetry, Remote Sensing and Spatial Information Sciences (ISPRS Annals). XXII ISPRS Congress, Melbourne, Australia, pp. 315–321.
Wang, A.H., Lettenmaier, D.P., Sheffield, J., 2011. Soil moisture drought in China, 1950–2006. J. Climate 24 (13), 3257–3271.
Wang, X.J., Zhang, J.Y., Shamsuddin, S., Amgad, E., He, R.M., Bao, Z.X., Ali, M., 2012. Water resources management strategy for adaptation to droughts in China. Mitigat. Adaptat. Strategies Global Change 17 (8), 923–937.
Wilhite, D.A., 2000. Drought: A Global Assessment, vol. 1. Routledge, New York.
Wilhite, D.A., Glantz, M.H., 1985. Understanding: the drought phenomenon: the role of definitions. Water Int. 10 (3), 111–120.
Wu, Z.Y., Lu, G.H., Wen, L., Lin, C.A., 2011. Reconstructing and analyzing China's fifty-nine year (1951–2009) drought history using hydrological model simulation. Hydrol. Earth Syst. Sci. Discuss. 8 (1), 1861–1893.
Yang, D.W., LI, C., Ni, G.H., Hu, H.P., 2004. Application of a distributed hydrological model to the Yellow River basin. Acta Geographica Sinica 59 (1), 143–154.
Yang, J., Gong, D., Wang, W., Hu, M., Mao, R., 2011. Extreme drought event of 2009/2010 over southwestern China. Meteorol. Atmos. Phys. 115 (3–4), 173–184.
Yang, P., Xiao, Z., Yang, J., Liu, H., 2013. Characteristics of clustering extreme drought events in China during 1961–2010. Acta Meteorol. Sin. 27 (2), 186–198.
Yevjevich, V., 1967. An Objective Approach to Definitions and Investigations of Continental Hydrologic Droughts. Colorado State University.
Yu, W., Shao, M., Ren, M., Zhou, H., Jiang, Z., Li, D., 2013. Analysis on spatial and temporal characteristics drought of Yunnan Province. Acta Ecol. Sinica 33 (6), 317–324.
Yu, M., Li, Q., Hayes, M.J., Svoboda, M.D., Heim, R.R., 2014. Are droughts becoming more frequent or severe in China based on the Standardized Precipitation Evapotranspiration Index: 1951–2010? Int. J. Climatol. 34 (3), 545–558.
Zhang, L., Xiao, J., Li, J., Wang, K., Lei, L., Guo, H., 2012a. The 2010 spring drought reduced primary productivity in southwestern China. Environ. Res. Lett. 7 (4), 045706.
Zhang, Q., Li, J.F., Singh, V.P., Bai, Y.G., 2012b. SPI-based evaluation of drought events in Xinjiang, China. Nat. Hazards 64 (1), 481–492.
Zhang, X., Wang, W.C., Fang, X., Ye, Y., Zheng, J., 2012c. Agriculture development-induced surface albedo changes and climatic implications across northeastern China. Chinese Geogr. Sci. 22 (3), 264–277.
Zhao, C., Deng, X., Yuan, Y., Yan, H., Liang, H., 2013. Prediction of drought risk based on the WRF model in yunnan province of China. Adv. Meteorol. 2013, 1–9.